BBA - General Subjects 1865 (2021) 129807

Contents lists available at ScienceDirect

BBA - General Subjects

journal homepage: www.elsevier.com/locate/bbagen

Curcumin rescue p53Y220C in BxPC-3 pancreatic adenocarcinomas cell line: Evidence-based on computational, biophysical, and in vivo studies

Lakshay Malhotra [a], Harsh K.V. Goyal [a], Sunita Jhuria [a], Kapil Dev [b], Saroj Kumar [a], Manoj Kumar [a], Punit Kaur [a], Abdul S. Ethayathulla [a,*]

[a] Department of Biophysics, All India Institute of Medical Sciences, New Delhi 110029, India
[b] Department of Biotechnology, Jamia Milia Islamia, New Delhi 110025, India

ARTICLE INFO

Keywords:
CD spectroscopy
Fluorescence spectroscopy
FTIR spectroscopy
Docking
Apoptosis
Annexin V/ PI

ABSTRACT

Background: The p53, tumor suppressor protein is inactivated upon mutation in the DNA-binding domain and the non-functional protein leads to cancers. The p53Y220C is one of the most frequently observed mutations in p53 with a scope of rescuing the protein function using small molecules.
Methods: Using computational modeling, biophysical, and experimental cell-based studies we tried to understand the molecular basis of Curcumin as a potential small molecule to stabilize p53Y220C mutant and restore its function. The pancreatic adenocarcinomas BxPC-3 p53Y220C mutant cell line was used for cell-based assays to determine the therapeutic potential of Curcumin to restore mutant p53 to function like wild type.
Results: Our results showed that the Curcumin binds p53Y220C with $K_d = 3.169 \pm 0.257$ μM and it increases the DNA binding affinity of the mutant by 4-fold with $K_d = 851.29 \pm 186.27$ nM. By Fluorescence, CD, and IR spectroscopy, we could characterize the secondary structural changes and stabilization of the p53Y220C DNA binding domain upon Curcumin binding. By caspase-3 and Annexin V assays, we could demonstrate that Curcumin at 3 μM to 8 μM concentration could initiate p53 mediated apoptosis in BxPC-3 cell line. Based on our experimental studies, we propose a mechanism for the activation of ATM/Chk1 kinases pathways for apoptosis and/or G2/M cell cycle arrest in the BxPC-3 cell line mediated by functionally restored p53Y220C.
Conclusion: The study indicated that the natural compound Curcumin could rescue mutant p53Y220C in BxPC-3 pancreatic adenocarcinomas cell line to function like wild-type and activate apoptotic pathways.

1. Introduction

Cancer cells exploit the mutation in p53 to heighten their growth and survival [1,2]. The non-functional p53 is the key determining factor in the uncontrolled proliferation of cells and in 85% of the human cancers, p53 was found to be with altered function [3–7]. Out of five functional domains of p53, the mutations are majorly observed in the DNA binding domain termed as a hotspot (DNA contact residues mutations) and non-hotspot mutations (structural mutations) [8,9]. Most of these mutations are missense mutations and specifically, the structural mutations lead to destabilization of protein. The oncogenic p53Y220C is one of the most frequently occurring p53 structural mutations with approximately 1,00,000 cases per year [2,8,10–14]. Pancreatic cancer is one of the cancers caused by p53Y220C with a 2 to 9% 5-year survival rate [15–18]. The structural mutant p53Y220C in the DNA binding domain leads to the loss of function and thermal stability of the protein [19,20]. The structural role of Tyrosine at 220th position on the periphery of the β-sandwich connecting strands S3/S4 and S7/S8 is to prevent the solvent entry into the hydrophobic core of the p53 DNA binding domain. The tyrosine residue form five electrostatic interactions among the backbone atoms of Val147, Pro151, Pro153, and Pro223 and holds the loops between β-strands S3/S4 and S7/S8 [21]. The mutation of Tyr220Cys results in the formation of a solvent-accessible crevice/cleft in the core domain structure [22]. Till now, various small-molecule ligands like Phikan083, PK5174, PK7088, and PRIMA-1 have targeted this cleft for the restoration of p53Y220C structure and function [16,23,24].

Curcumin used as a traditional medicine in India exhibit enormous therapeutic potential against human diseases. Many clinical trials of Curcumin have been reported against various cancers like colorectal cancer [25,26], breast cancer [27], multiple myeloma [28], pancreatic

Abbreviations: p53wt, p53 DNA binding domain wild type; p53Y220C, p53Y220C DNA binding domain; IPTG, Isopropyl-1-thio-β-d-galactopyranoside.

* Corresponding author.
E-mail address: ethayathulla@aiims.edu (A.S. Ethayathulla).

https://doi.org/10.1016/j.bbagen.2020.129807
Received 18 September 2020; Received in revised form 19 November 2020; Accepted 26 November 2020
Available online 2 December 2020

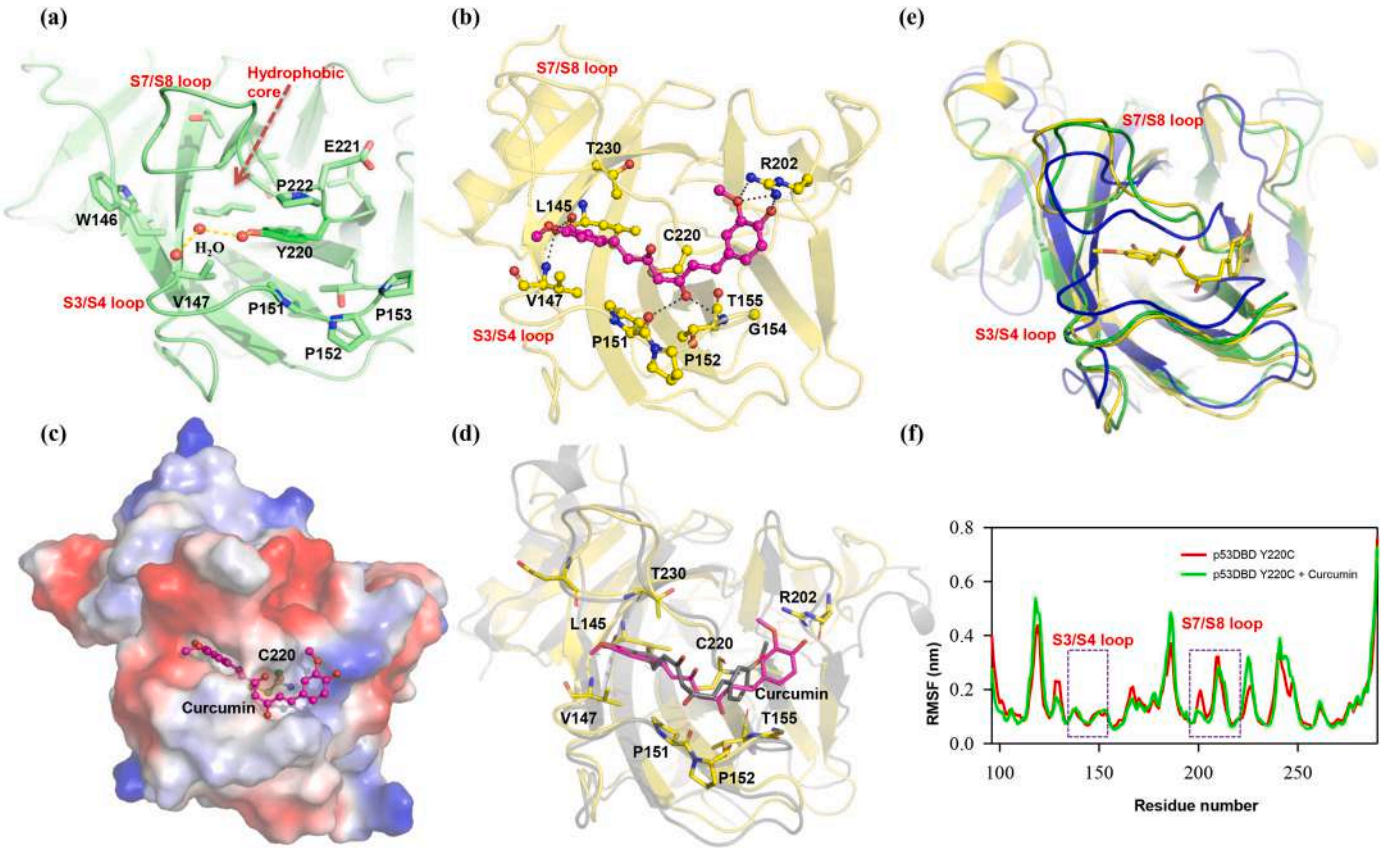

Fig. 1. Structure of p53 DNA binding domain. (a) p53wt: The hydrophobic core, solvent molecules interactions, and the residues lining the entry of the hydrophobic are shown in ball and stick (b) p53Y220C: The interactions of docked Curcumin with the residues of p53DBD is shown. (c) The electrostatic surface potential of p53Y220C with docked Curcumin buried inside the crevice. (d) Superimpose of p53Y220C docked with Curcumin before and after 100 ns MD simulations.

cancer [29,30], and other cancers. A promising strategy for the development of novel p53 anticancer therapy is by the reactivation of the mutant tumor suppressor with small molecules/ligands. Recent studies reported ethyl amide small molecule analog MB725 [31] binds p53Y220C and stabilizes p53Y220C with cytotoxicity IC_{50} values of 18 μM. Compounds like PK083, PK7088, and PK5196 were shown to bind p53Y220C with cytotoxicity IC_{50} values of 43, 57, and 11 μM, respectively [24,31–34]. The cytotoxicity of all the compounds reported so far was measured after 72 h of drug treatment except PRIMA-1, with cytotoxicity of 68.7 μM after 24 h of treatment [35]. In this study, we attempted to explore the therapeutic potential of Curcumin against p53Y220C genomic mutant human pancreatic adenocarcinoma cell line. We have performed computational modeling, biophysical studies to monitor the Curcumin-induced secondary structural changes in p53wt and p53Y220C using spectroscopic techniques (CD, Fluorescence, and IR). We have performed cell-based functional assays to validate the role of Curcumin to restore the mutant p53 to activate pathways of apoptosis in the BxPC-3 (human pancreatic cancer) cell line.

Table 1
Interactions formed between p53Y220C and Curcumin.

S.No.	Interactions		Before MD	After 100 ns MD simulations
	Protein	Curcumin	Distance	Distance
1.	Val 147 NH	O4'	2.5 Å	2.6 Å
2.	Pro151 O	OH2	3.5 Å	3.2 Å
3.	Pro152 O	OH2	2.8 Å	–
4.	Thr155 NH	O2	2.5 Å	2.9 Å
5.	Leu145 O	OH4'	2.8 Å	2.5 Å
6.	Arg202 NH1	O4	2.4 Å	–
7.	Arg202 NH1	O3	2.4 Å	–
8.	Arg202 NH2	O3	2.5 Å	–
9.	Cys220 NH	O4	–	2.9 Å

2. Materials and methods

2.1. Cloning, expression, and purification of p53wt and p53Y220C mutant

The p53wt was PCR amplified from the p53 full length cloned in pCEP4 vector provided by Dr. Sanjeev Das, National Institute of Immunology. The amplified gene was cloned in a pET-28a (Promega, USA) expression vector with a C-terminal His_6 tag. The p53Y220 mutant was generated by site-directed mutagenesis using p53wt DBD plasmid. Both the p53DBD plasmids were isolated after transformation in DH5α cells sequenced for confirmation.

2.2. Expression and purification of p53wt and p53Y220 mutant

The p53DBD constructs transformed into *E. coli* BL21(DE-3) strain for the protein expression. Cells were initially grown in 10 mL LB culture supplemented with 50 μg/mL kanamycin at 37 °C. Cultures were grown till absorbance reached ~0.6 at 600 nm and induced with 0.5 mM IPTG at 18 °C for 12 h. The cells were harvested by centrifugation at 3800 rpm for 15 min and frozen at −80 °C. The cell pellet resuspended and lysed by freeze-thaw followed by sonication in lysis buffer containing 20 mM Sodium citrate pH 6.5, 500 mM NaCl and 10% Glycerol, and 10 μM $ZnCl_2$. The clear supernatant after centrifugation at 12000 rpm for 30 min was loaded with 2 mL Ni-NTA resin (GE) and kept for batch binding at 4 °C. The protein-bound resin was washed twice with 20 mL of buffer containing 5

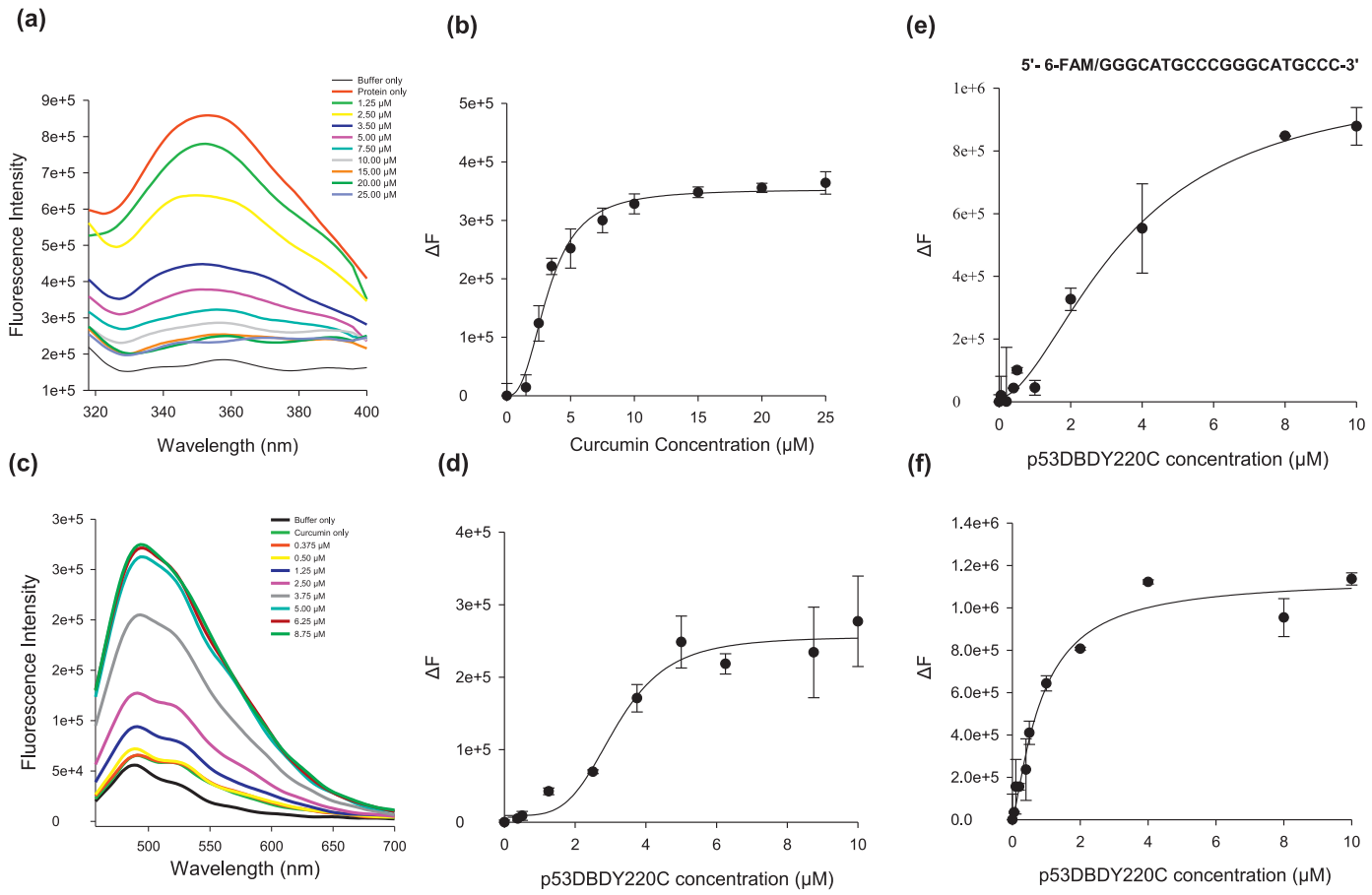

Fig. 2. DNA and Curcumin binding studies with p53Y220C by Fluorescence Spectroscopy. (a) Tryptophan quenching assay spectra with a fixed concentration of p53Y220C and varying Curcumin concentration from 1 to 25 μM. (b) The Tryptophan quenching Curcumin binding curve (c) Curcumin fluorescence binding assay spectra with a fixed concentration of Curcumin and varying concentration of p53Y220C from 0.375 to 8.75 μM (d) The fluorescence Curcumin binding curve (e) and (f) FAM-labeled DNA binding assay with p53Y220C in (e) absence of Curcumin and (f) presence of 1:4 Curcumin concentration.

mM and 20 mM imidazole, respectively. The p53wt and p53Y220C proteins were eluted with 20 mM Sodium citrate pH 6.5, 150 mM NaCl, 300 mM imidazole, 10 μM $ZnCl_2$. Further purification was carried out using size exclusion chromatography using Superdex 200 HiLoad 26/600 column (GE Healthcare Life Sciences) in buffer 20 mM Sodium citrate pH 6.5, 150 mM NaCl and the purity analyzed using 15% SDS-PAGE.

2.3. Computational modeling studies

The Crystal structure of p53Y220C [PDB ID:6SHZ_A] [17] was used for docking studies after removing the solvents and energy minimization. The binding site was defined at the crevice formed between β-strands S3/S4 loop and β-strands S7/S8 loop along with the residues governing the cleft including Cys220. The Curcumin ligand coordinates were obtained from Protein Databank (PDB ID:5ZTN) [36] and energy minimized before docking. Molecular docking of prepared Curcumin in the defined binding site of p53Y220C was performed by AutoDock 4.2.6 [37] using docking parameters as described in previous studies [38,39]. In the top 50 docked poses, the conformations with the lowest free energy of binding in the largest cluster was selected as the best-docked conformation of Curcumin. The selected docked conformation of the Curcumin with p53Y220C was energy minimized and refined by molecular dynamics (MD) simulations. MD simulation of the complex was performed using GROMACS-5.0.7 [40] with the help of forcefield parameters of GROMOS 54a7 [41,42] similar to previous studies [43]. A cubic box (10 Å in each direction from protein atoms) was generated and the docked complex was solvated using the SPC216 water model and the system was neutralized with Cl^- ions. The solvated complex was energy minimized by the steepest descent algorithm with convergent criteria of less than 1000.0 kJ/mol/nm and subjected to 100 ns MD simulation at 300 K and 1 atm pressure for 100 ps using Berendsen thermostat and Parrinello-Rahman barostat in Periodic Boundary Condition. The position and velocity of atoms were integrated using Leapfrog Dynamics integrator at the step size of 1 fs, all bonds were constrained with the LINCS algorithm. Long-range electrostatic forces were calculated by Particle Mesh Ewald (PME) algorithm while the cut-off scheme was used for short-range forces using the Verlet scheme for neighbour searching. The same protocol was used for MD simulations of p53Y220C in the absence of Curcumin for comparative study.

2.4. CD spectroscopic analysis

The Far-UV spectrum was monitored over a wavelength range of 200–250 nm using JASCO J-1500 CD Spectrophotometer using a 0.1 cm path length quartz cuvette. The CD spectra were taken in two sets using 20 mM phosphate buffer containing 10 μM $ZnCl_2$, one set with p53Y220C in absence of Curcumin, and another set protein incubated with 60 μM Curcumin (Sigma Aldrich PCode:1002542749) for 30 min at 4 °C. The CD spectra were also measured for both the protein samples

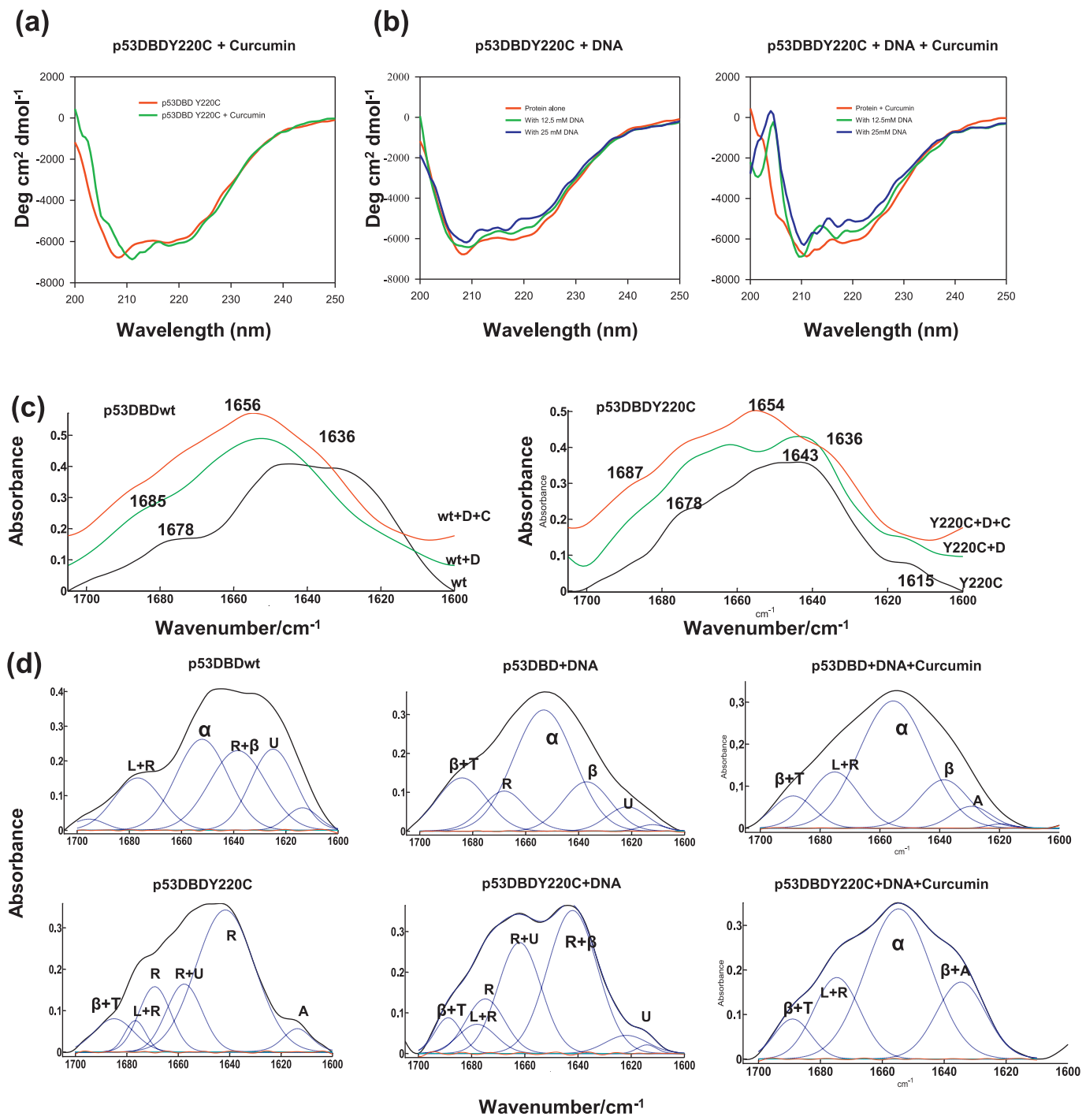

Fig. 3. The CD spectra of p53Y220C with DNA and Curcumin. (a) CD spectra of 12.5 μM p53Y220C in the absence (red) and presence (green) of 60 μM Curcumin. (b) CD thermal spectra of p53Y220C in the absence (red) and presence (green) of Curcumin. (c) The left panel shows the CD spectra of p53Y220C in the absence (red) and presence of 12.5 μM (green) and 25 μM (blue) 13 bp DNA. The right panel shows the CD spectra of p53Y220C in the presence of Curcumin respectively. (d) and (e) The IR spectra of p53wt and p53Y220C with DNA and Curcumin. (d) The left panel shows the IR spectra of p53wt, p53wt with 20 bp DNA, p53wt + 20bpDNA + Curcumin and the right panel shows IR spectra of p53Y220C, p53Y220C with 20 bp DNA, p53Y220C + 20bpDNA + Curcumin. (e) The IR spectra show the change in the secondary structure of p53wt (top panel) and p53Y220C (bottom panel).(For interpretation of the references to color in this figure legend, the reader is referred to the web version of this article.)

with 12.5 μM and 25 μM of DNA (5′-CGGGCATAGCCCG-3′). An average of 2 scans was taken for each spectrum. The spectral scans were also taken immediately after adding for both p53Y220C with or without 60 μM Curcumin. The CD spectra were plotted using Sigma plot 10.0 and the secondary structure was calculated using the online server BESTSEL [44,45].

2.5. FT-IR spectroscopic analysis

The Fourier Transform Infra-Red (FTIR) measurements of (i) p53wt (80 μM of 200 μl), (ii) p53Y220C (40 μM of 200 μl), (iii) p53wt and p53Y220C with 20 bp DNA (20 bp: 5′-CGGGCATGCCCGGGCATGCCCG-3′) (1:5 of 200 μl), (iv) p53wt and p53Y220C with Curcumin and (v) p53Y220C with 1:5 ratio of DNA in the presence of Curcumin were

Table 2
Secondary structure content analysis of p53Y220C using CD spectroscopy.

p53Y220C	Secondary structure content			
	α-helix	β-sheet	Random coil	NRMSD
p53DBD Y220C (12.5 μM)	7.2	35.3	57.5	0.026
p53DBD Y220C + 12.5 μM DNA	6.9	34.8	58.4	0.027
p53DBD Y220C + 25 μM DNA	5.0	36.0	59.1	0.027
p53DBD Y220C + 60 μM Curcumin	10.1	34.5	55.4	0.031
p53DBD Y220C + 60 μM Curcumin + 12.5 μM DNA	8.0	38.9	53.1	0.072
p53DBD Y220C + 60 μM Curcumin + 25 μM DNA	7.4	40.0	52.6	0.045
Crystal structure of p53DBDwt	10	34	56	–

performed. All the FTIR measurements were done at 4 cm^{-1} spectral resolution using Bruker Vertex 27 FTIR spectrometer combined with attenuated total reflection elements (ATR) equipped with a DTGS detector and N_2 gas purging system at room temperature. The protein samples were prepared in buffer 20 mM Sodium citrate pH 6.5 with 10 μM $ZnCl_2$ and a total of 100 spectral scans were measured ratioed against 200 scan background spectra in the range in the 4000–900 cm^{-1} region. Three individual experiments were performed for each sample using the OPUS (Bruker, Germany) spectrometer software at room temperature. To estimate the secondary structure content, curve fitting was performed in the amide I region. Before the curve fitting, the baseline was corrected by the least square curve fitting method using the Kinetics program [46]. The second derivative spectrum was used to determine the initial peak positions for curve fitting.

2.6. Tryptophan quenching assay

The Curcumin binding to p53Y220C was measured using a tryptophan quenching assay. The assay was performed with 5 μM p53Y220C in the buffer 20 mM Sodium citrate pH 6.5, 150 mM NaCl and 10 μM $ZnCl_2$ incubated with different concentrations of Curcumin from 0 to 25 μM at 4 °C for 30 min. The samples were excited at 295 nm and the emission spectra from 320 to 400 nm measured for each Curcumin concentration [47]. The experiments were performed in triplicates and the spectral reading was recorded using Spectramax i3x microplate reader. The spectra analysis and K_d were determined using Sigmaplot 14.0.

2.7. Curcumin binding assay

The Curcumin binding to p53Y220C was also measured using the emission maxima of Curcumin at 495 nm after exciting at 425 nm [48]. The assay was performed using 0.5 μM Curcumin in the 20 mM Sodium HEPES buffer pH 7.5 along with 100 mM sodium chloride and 10 μM $ZnCl_2$ with different p53Y220C protein concentrations from 0 to 10 μM in the same buffer, with the incubation period of 30 min at 4 °C. The samples were excited at 425 nm and the emission spectra were measured from 450 to 700 nm for each protein concentration. The experiment was performed in triplicates and the Spectramax i3x microplate reader was used for measuring the spectral readings [48–50]. The spectral measurements and the K_d were determined using Sigmaplot 14.0.

2.8. p53Y220C and 6-FAM DNA binding assay

The binding of p53Y220C to 6-FAM labeled DNA in the presence and absence of Curcumin was examined using the excitation and emission of 6-FAM labeled DNA (495 / 530 nm). The fluorescence DNA binding study was done with a similar protocol described in [92]. A 20 nM of 20-mer 6-FAM DNA (5′-6-FAM/GGGCATGCCCGGGCATGCCC-3′) was titrated on different p53 Y220C concentrations ranging from 50 nM to 10 μM with or without Curcumin. The stoichiometry of protein:ligand was 1:4 and all the dilutions were performed in 20 mM Sodium citrate buffer pH 6.5 containing 150 mM NaCl and 10 μM $ZnCl_2$. The experiment was performed in duplicates with a reaction volume of 100 μL. The protein was incubated with Curcumin for 30 min at 4 °C and then 20 nM of 6-FAM-DNA was added and again subjected for incubation at 4 °C for 30 min followed by fluorescence measurement using Spectramax i3x and finally, the graphs were plotted in Sigmaplot 14.0. The binding of p53wt to 6-FAM labeled DNA was also performed using the excitation and emission of 6-FAM labeled DNA (495 / 530 nm) and a graph was plotted for determining K_d.

2.9. Cell culture

The Human pancreatic p53Y220C mutant cancer line BxPC-3 was purchased from the ATCC, Manassas, VA, USA. Cells were frozen in −80 °C and LN_2 in multiple vials and cultured (described below) for less than 20 population doublings for the present study. The cells were cultured in RPMI-1640 Media (Gibco, Thermo Fisher Scientific) along with 10% Fetal bovine serum (South American Origin, Gibco) and 1% Antibiotic- Antimycotic(100×) (Gibco). Cells were maintained in Thermoscientific humified incubator at 37 °C with 5% CO_2 (LEGENDRE, SOOKDEO, and FOSTER 2014). Cell disassociation for cell passaging was done with the 1× Trypsin 0.25% and 0.2% EDTA in Dulbecco's phosphate-buffered saline (Himedia). All the cell-based experiments were performed between 7 and 13 passages.

2.10. Immunofluorescence

About 0.3 × 10^6 BxPC-3 cells were seeded on polylysine treated coverslips in 6 well plates with 2 mL of complete RPMI media. When the confluency reached 60–70%, cells were treated with 100% methanol (chilled at −20 °C) for 5 min followed by permeabilization using 1× PBS and 0.05% Triton X 100 for 10 min and then washed with PBS for 5 min. Then the cells were blocked for 30 min using 2% skimmed milk in PBST (PBS + 0.1% Tween-20) and incubated with FITC labeled p53 monoclonal antibody (Mouse / IgG2a Invitrogen (BP53–12) in PBST (1:300 dilution) for overnight at 4 °C. After washing with PBS, the cells were incubated with 0.5 μg/mL DAPI (Invitrogen) for 2 min [51]. Finally, the coverslip was rinsed with PBS and put on a glass slide and visualized under the fluorescence microscope (Nikon, Eclipse Ti) using FITC and DAPI filter [52].

2.11. Cell viability assay

The human pancreatic BxPC-3 cells seeded approximately 8000 cells per well-grown in a 96 well plate for 24 h in media (RPMI 1640, 10% FBS, 1% Antibiotic and Antimycotic). The cells were treated with different concentrations of Curcumin from range 0 to 10 μM for the next 24 h. The cell viability for both control and Curcumin-treated cells determined by MTT (3-(4,5-Dimethylthiazol-2-yl)-2,5-Diphenyltetrazolium Bromide) (Molecular Probes, Invitrogen). As per standard protocol, cells were incubated with MTT (0.5 mg/mL in PBS) at 37 °C, incubated at 5% CO_2 for 4 h. The MTT was replaced with 80 μL DMSO and the absorbance for the blue formazone crystals was measured at 575 nm using SpectraMax i3x. The assay was performed in six replicates and the IC_{50} with standard deviation obtained using Sigmaplot 14.0. The cytotoxicity percentage was calculated using the equation given below [53].

$$Cytotoxicity\ Percentage = \left(\frac{1 - Absorbance\ of\ sample}{Absorbance\ of\ negative\ control}\right)100$$

2.12. Comet assay

The DNA Comet assay was performed to detect the DNA-Double strand breaks by following the instructions from the Comet SCGE assay kit (ADI-900-166, Enzolifesciences) using the TBE electrophoresis

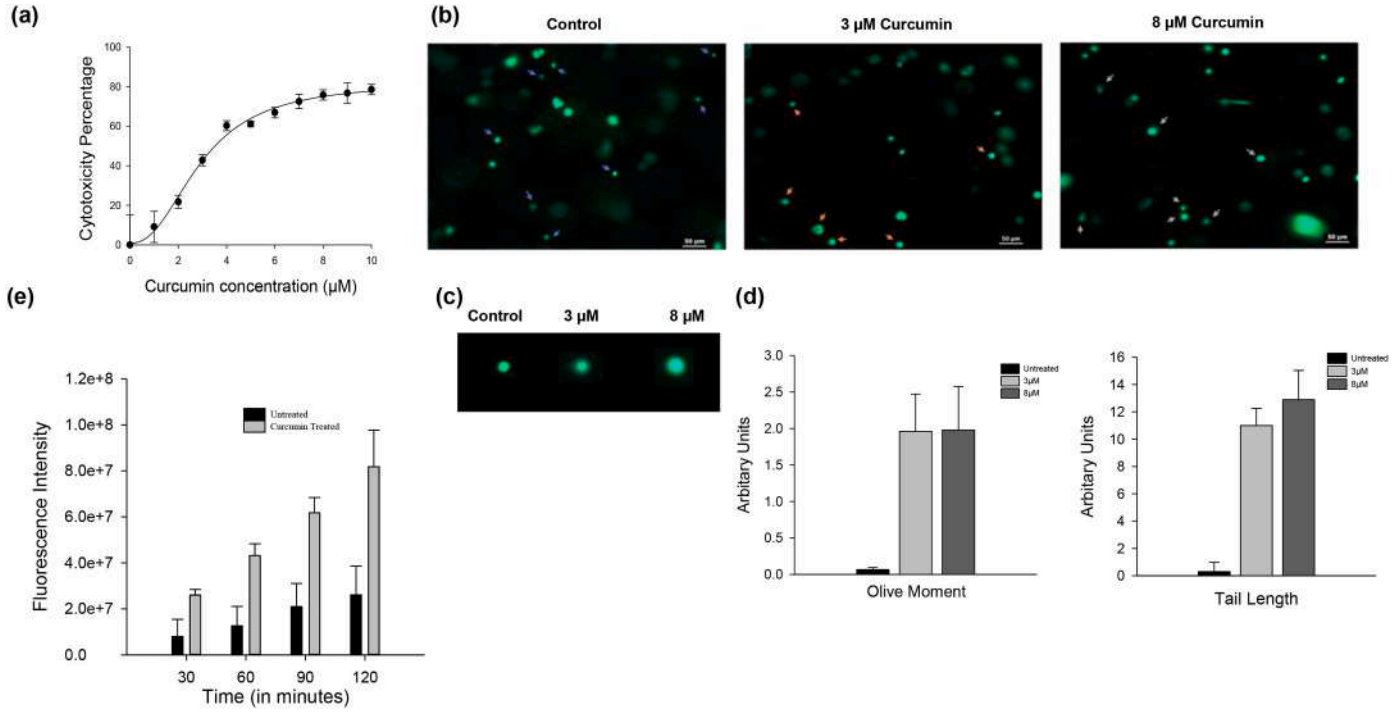

Fig. 4. The MTT and COMET assay of Curcumin in the BxPC-3 cell line. (a) The cytotoxicity with increasing concentration of Curcumin in BxPC-3 cell line after 24 h drug treatment. (b) COMET assay of BxPC-3 cell lines after treatment with 3 μM and 8 μM Curcumin. (c) represents the change in cell shape after Curcumin treatment (d) The bar diagram shows the change in the olive moment and tail length observed from a total of 10 comets from each group. The COMETs were analyzed using OpenComet software. (e) Analysis of caspase-3 activity assay in Curcumin-treated BxPC-3 cell line. Cells were pre-treated with 8 μM Curcumin for 24 h and caspase-3 activity was measured at different time intervals.

method. BxPC-3 cells were treated with 0, 3 and 8 μM doses of Curcumin prepared and the comet assay was performed [54–56]. The comet analysis for 10 comets was done using the opencomet plugin of ImageJ and the graph was plotted using Sigma Plot [57–59].

2.13. Annexin V and PI staining microscopic

The apoptotic cell bodies upon Curcumin treatment in BxPC-3 cell lines were detected using Annexin V (Alexa fluor 488 conjugated) /PI double staining kit (Invitrogen) analyzed under microscopic images. The BxPC-3 1×10^6 cells seeded in a 6-well plate treated with 3 μM, and 8 μM Curcumin concentration for 24 h were analyzed under Nikon Eclipse Ti microscope and the images captured at different conditions. The cells were trypsinized and washed with ice-cold 1× PBS buffer centrifuged at 1200 rpm for 5 min at room temperature. The Annexin V staining was done as per the protocol described in the manual. A 10 μL of Annexin conjugate and 1 μL of 100 μg/mL of PI (dissolved in 1× Annexin buffer) added to each 100 μL of cell suspension and incubated for 15 min at room temperature. After incubation, the cells were washed and resuspended in annexin buffer and were used to prepare slides to visualize under a fluorescence microscope. The FITC and TRITC filters were used for visualizing the Alexa flour 488 conjugated Annexin and PI staining respectively [60,61].

2.14. Caspase-3 assay

The p53 mediated apoptosis was detected by assaying the increase in caspase-3 activity in Curcumin-treated BxPC-3 cell lines. Approximately 0.1×10^6 cells per well seeded in a 12 well plate containing complete RPMI medium. The next day, cells were treated with 8 μM Curcumin for 24 h at 37 °C with 5% CO_2. The cells were then harvested, washed with PBS, lysed, and caspase-3 activity was analyzed using the EnzCheck Caspase-3 Assay Kit #1 (Invitrogen, Life Technologies, Waltman, MA, USA) according to the protocol in the instruction sheet [62–65]. The assay was performed in triplicatess and the fluorescence intensity was measured at 441 nm for 30, 60, 90, and 120 min of incubation after exciting the sample with 342 nm using Spectramax i3x.

3. Results

3.1. Computational modeling of Curcumin with p53Y220C

The overall fold of the DNA binding domain of p53 family proteins; p53 [66,67], p63 [68], and p73 [69,70] are similar. The role of the core domain (92–293) is to recognize the decameric consensus DNA sequence of PPPCA/TGYYY explicitly (where P = A or G, and Y = C or T) having the spacing of 0 to 13 base pairs. The domain forms an immunoglobulin-like anti-parallel beta-sandwich and the protein recognizes DNA by the loop-sheet-helix motif [67] (Fig. 1a, S1a).

The core domain recognizes DNA bases by the structural rearrangement of the motif loop L1, helix H2, and β-strand S10. The mutant p53Y220C also forms a similar fold with no variations observed from wild type [9]. The mutation of Tyr220 to Cysteine leads to the formation of an extended surface crevice between the loops S3/S4 and S7/S8 (Fig. S1a). The role of tyrosine 220 was to stabilize the loops through a network of water-mediated interactions with the backbone atoms of the loops [17]. Upon mutation, the solvent accessibility increases, as a result, the domain gets destabilized with a decrease in thermal stability 4 kcal/mol [1,2]. The crevice solvent accessible area increases to ~681 $Å^2$ compared to p53wt ~ 664 $Å^2$ (Fig. S1a) [71]. The ligand Curcumin was docked to p53Y220C mutant at the same site as observed in the structure complex of Phikan derivatives [15,31]. The Curcumin occupies the surface crevice by forming six hydrogen-bonded interactions with the backbone atoms of Leu145, Val147, Pro151, Pro152, Thr155,

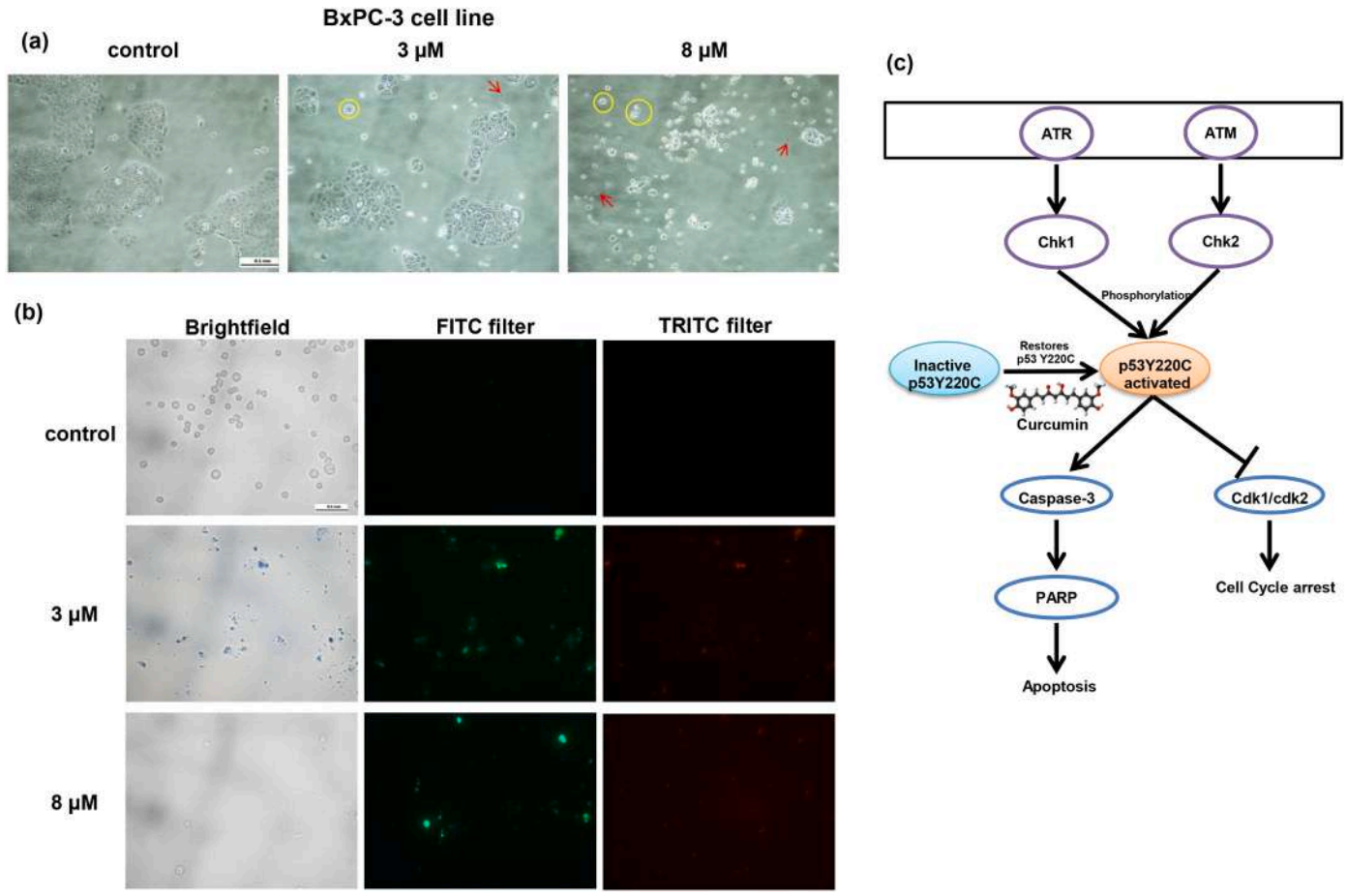

Fig. 5. Annexin V and PI staining of BxPC-3 cell line and proposed p53Y220C apoptotic pathway. (a) Microscopic image of BxPC-3 cell line after 24 h treatment with 3 μM and 8 μM Curcumin concentration. The yellow circles indicate the blebbing and the red arrow indicates apoptotic bodies (b) Fluorescent analysis of BxPC-3 cells, untreated, 3 μM Curcumin treatment, 8 μM Curcumin treatment using Annexin V-FITC (green) and Propidium Iodide (red). Cells possessing early apoptotic phase appear green on FITC filter and cells in late apoptotic phase appear in both green and red in FITC and TRITC filter. (c) The proposed apoptotic pathway of functionally restored p53Y220C by Curcumin.

and side-chain of Arg202 (Fig. 1b) (Table 1).

The docked p53Y220C complex with Curcumin subjected to 100 ns MD simulations showed that the ligand was stable throughout the simulation with five hydrogen-bonded interactions with the backbone atoms of residues Leu145, Val147, Pro151, Thr155, and Cys220 (Fig. 1c–d). A comparison of the MD trajectory of p53Y220C in the absence and presence of Curcumin showed that the loop S3/S4 and S7/S8 of the complex were more stable in the presence of Curcumin than the native protein (Fig. 1e and f).

3.2. Curcumin binding

The binding affinity of Curcumin with p53Y220C measured using the fluorescence binding assay [49] with the intrinsic tryptophan 146 quenching by varying Curcumin concentrations (1 μM to 25 μM). The decrease in intrinsic fluorescence with an increase in Curcumin concentration indicates the binding of the ligand to p53Y220C. Based on the quenching assay, the measured K_d was found to be 3.23 ± 0.207 μM (Fig. 2a and b).

The Curcumin binding was further validated by fluorometric titration assay, where the change in Curcumin fluorescence upon protein binding was monitored at 495 nm [48,50]. Curcumin at 0.5 μM concentration showed weak fluorescence and upon addition of p53Y220C, the fluorescence of Curcumin increased significantly and saturated at 8.75 μM. The K_d calculated based on the fluorometric titration assay was found to be 3.169 ± 0.257 μM (Fig. 2c and d). Both fluorescence assays establish that Curcumin binds p53Y220C with K_d of ~3 μM.

3.3. DNA binding studies by fluorescence spectroscopy

The DNA binding affinity of p53wt, p53Y220C in the absence and presence of Curcumin were performed using 21 bp 6-FAM labeled DNA by measuring the change in the fluorescence with constant DNA and increasing protein concentration [72]. The p53wt binds 21 bp DNA promoter sequence with K_d of 70.667 ± 13.662 nM (Fig. S2a) and p53Y220C shows affinity with K_d value of 3555.19 ± 721.86 nM (Fig. 2e). Interestingly, upon incubation of p53Y220C with Curcumin the binding affinity of protein towards DNA sequence increased by 4-fold with K_d of 851.29 ± 186.327 nM (Fig. 2f). The binding of Curcumin to the crevice in the DNA binding domain provides the plasticity required by p53 to bind DNA. The CD and IR spectroscopy analysis was performed to understand the secondary structural changes in p53Y220C both in the absence and presence of DNA and Curcumin.

3.4. CD spectroscopy measurements

Circular Dichroism is an excellent tool to determine the secondary structure of proteins upon binding to DNA/ligands by measuring the optical transitions. The native CD spectra of p53Y220C and the change in absorbance upon binding to DNA in the presence and absence of

Table 3a
Distance between the S3/S4 and S7/S8 loops in p53Y220C at different frames in the MD simulations in the presence of Curcumin.

Time (ns)	Distance between the residues (in Å)					
	T155-C220	E221-P152	P222-T150	G226-S149	D228-D148	W146-C229
0	5.8 Å	10.8 Å	8.3 Å	16.8 Å	10.4 Å	5.7 Å
10	5.7 Å	10.6	11.9 Å	13.3 Å	9.5 Å	5.6 Å
20	6.3 Å	10.5 Å	8.1 Å	15.3 Å	13.6 Å	5.8 Å
30	6.0 Å	12.3 Å	9.5 Å	14.6 Å	10.6 Å	5.9 Å
40	7.1 Å	11.0 Å	9.2 Å	14.4 Å	10.0 Å	5.4 Å
50	5.5 Å	11.2 Å	10.1 Å	19.0 Å	10.7 Å	5.3 Å
60	5.5 Å	10.9 Å	9.1 Å	19.0 Å	12.3 Å	6.2 Å
70	5.8 Å	11.5 Å	9.3 Å	16.2 Å	9.8 Å	5.5 Å
80	5.7 Å	11.5 Å	9.5 Å	16.4 Å	11.2 Å	5.4 Å
90	5.9 Å	11.0 Å	9.3 Å	17.9 Å	10.6 Å	5.3 Å
100	6.8 Å	11.4 Å	9.1 Å	17.4 Å	9.9 Å	5.0 Å

Table 3b
Distance between the S3/S4 and S7/S8 loops of p53Y220C during MD in the absence of Curcumin.

Time (ns)	Distance between the residues (in Å)					
	T155-C220	E221-P152	P222-T150	G226-S149	D228-D148	W146-C229
0	5.7 Å	10.8 Å	7.5 Å	16.6 Å	10.5 Å	5.3 Å
10	5.9 Å	9.9 Å	6.8 Å	8.9 Å	10.0 Å	4.6 Å
20	5.8 Å	9.9 Å	8.2 Å	9.0 Å	10.2 Å	5.0 Å
30	5.5 Å	9.7 Å	8.2 Å	9.4 Å	10.9 Å	4.9 Å
40	5.6 Å	10.4 Å	7.0 Å	8.8 Å	11.6 Å	5.0 Å
50	5.5 Å	10.5 Å	8.3 Å	9.5 Å	11.8 Å	5.1 Å
60	5.9 Å	10.0 Å	7.4 Å	9.7 Å	11.0 Å	5.1 Å
70	6.2 Å	10.9 Å	8.6 Å	9.9 Å	11.2 Å	5.0 Å
80	5.5 Å	9.5 Å	6.8 Å	10.3 Å	13.4 Å	6.8 Å
90	5.5 Å	10.0 Å	8.2 Å	9.7 Å	12.3 Å	5.6 Å
100	5.7 Å	10.6 Å	8.8 Å	9.7 Å	11.2 Å	4.8 Å

Curcumin was measured. The p53Y220C showed a peak at 218 nm for the β-sheet in spectra but not prominent. Upon addition of Curcumin, the protein gets stabilized and prominent secondary peaks of π to π*transitions and n to π*transitions appeared in the CD spectra at 208 nm and 222 nm for β-sheets respectively [73–75]. The distinct shift of n to π*transitions in the spectra at 208 nm to 215 nm indicates the structural rearrangement upon CCurcumin binding to p53Y220C (Fig. 3a).

3.5. CD spectra in the presence of DNA and Curcumin

The CD measurements of p53Y220C with DNA in an increasing concentration from 12.5 μM to 25 μM showed no significant change in spectra (Fig. 3a). Whereas, a definite band with an increase in magnitude observed between 200 and 205 nm and a decrease in negative ellipticity absorption at 222 nm in the spectra indicates the secondary structural change in p53Y220C mutant upon binding DNA with Curcumin (Fig. 3b). The change in absorption and the protein secondary structural changes in the p53Y220C DNA complex supports that Curcumin stabilizes the protein and increases its affinity for DNA (Table 2).

3.6. IR spectroscopy measurements

The IR spectroscopy is a label-free biophysical technique that provides information about the secondary structure elements and changes observed upon DNA or ligand binding to the protein [76,77]. The IR spectrum from 1700 to 1600 cm^{-1} provides information of protein secondary structure contents like α-helix in the region 1660–1650 cm^{-1}, β-sheets from 1640 to 1630, and 1695–1680 cm^{-1}, loop/random coils from 1686 to 1662 cm^{-1} and the disordered regions from 1650 to 1640 cm^{-1}. This is the first IR spectral study to be reported for p53wt and p53Y220C for native and in presence of DNA and ligand. The IR spectra of p53wt and p53Y220C in the presence of DNA and Curcumin showed the changes in the secondary structural content upon binding.

3.7. IR spectra of p53wt in the presence of DNA and Curcumin

The native p53wt and p53Y220C DNA binding domain majorly consist of 34% β-sheets and 10% α-helices. In the IR spectra of native p53wt (Fig. 3c), four characteristic bands at 1678 cm^{-1} (random coil/loop), 1648 cm^{-1} (disordered/random coil), 1635 cm^{-1} (β-sheets) and 1629 cm^{-1} (unstructured). The spectra of p53wt incubated with DNA showed the changes in secondary structure with bands at 1685 cm^{-1} for anti-parallel β-sheets/turns, 1656 cm^{-1} for α-helices, and 1636 cm^{-1} for β-sheets indicating that the protein gets stabilized upon binding DNA (Fig. 3c). Interestingly the spectra of p53wt in presence of Curcumin further sharpen the band at 1656 cm^{-1} (α-helices) and 1636 cm^{-1} (β-sheets) indicating more ordered conformation of the protein [46].

3.8. IR spectra of p53Y220 in the presence of DNA and Curcumin

The IR spectra of p53Y220C showed a significant difference in comparison to p53wt (Fig. 3d). In the spectra of p53Y220C, three characteristic bands at 1678 cm^{-1} (random coils/loops), 1643 cm^{-1} (random coils/disordered) and 1615 cm^{-1} (unstructured) were observed. A prominent band at 1678 cm^{-1}indicates the presence of large unstructured loops and coils in the protein compared to p53wt [77]. The appearance of the band of the unstructured loop at 1678 cm^{-1} may be the result of the destabilizing solvent into the hydrophobic core [76]. In the spectra of p53Y220C with DNA, two new bands appeared at 1661 cm^{-1} (random coils/α-helices) and 1639 cm^{-1} (mix of the random coil and β-sheets). A shift of 1678 cm^{-1} band to 1661 cm^{-1} and 1643 cm^{-1} to 1639 cm^{-1} (Fig. 3d) indicatethat the structural changes upon binding to DNA but not in ordered conformation in comparison to the spectra of p53wt with DNA (Fig. 3c).

Interestingly, in the IR spectra of Curcumin bound p53Y220C with DNA (Fig. 3d), bands appeared at 1686 cm^{-1} (antiparallel β-sheets/turn), 1654 cm^{-1} (α-helices), and 1636 cm^{-1} (β-sheets). These changes in spectra are like the changes observed with p53wt + DNA + Curcumin indicates that the p53Y220C in the presence of Curcumin binds DNA with greater affinity as observed from fluorescence DNA binding assay. The spectra of p53Y220C with Curcumin in the absence of DNA (Fig. S2b), bands at 1652 cm^{-1} (α-helices), and 1636 cm^{-1} (β-sheets) [76,77] were observed, indicating the binding of Curcumin increases stability in p53Y220C (Fig. 3d). The CD spectra of p53Y220C with DNA also showed similar results with a peak at 216 nm in the presence of Curcumin absent in the spectra of both protein alone and protein with DNA.

3.9. MTT cytotoxicity assay

The experimental studies with Curcumin performed using the human pancreatic cancer cell line (BxPC-3) harboring p53Y220C mutation in the genome [35,78,79]. The expression of p53Y220C in the human pancreatic cancer cell line was analyzed by immunofluorescence (Fig. S2c) using FITC and DAPI filters under the fluorescence microscope. Dose-dependent effect of Curcumin in BxPC-3 cell line was done by MTT assay. The dose-response showed an IC_{50} value of ~3 μM (3.30 μM) after 24 h of treatment of BxPC-3 cell line with Curcumin (Fig. 4a).

The COMET assay was performed with 3 μM (50% cytotoxicity) and 8 μM (70% cytotoxicity) dose concentration to observe apoptosis. The comet assay slides of the BxPC-3 cell line were prepared using 3 and 8 μM concentrations of Curcumin along with negative control. A total of 10 comets from each group were analyzed using open comet software and the comets in 3 μM and 8 μM slides appear with the more significant olive moment and long-tail length in comparison to the negative control

(Fig. 4b–d). The assay indicates that Curcumin induces apoptosis in the BxPC-3 cell line.

3.10. Caspase-3

To detect the apoptosis in BxPC-3 cell line in the presence of Curcumin, caspase-3 assay performed for 8 μM dose concentrations along with negative control [62,64,80]. The Curcumin treated cells showed very high fluorescence intensity as compared to the negative control. The increase in fluorescence intensity reflects the increase in the Caspase-3 production, which utilizes the DEVD-AMC substrate and AMC will be released. An increased caspase-3 activity was observed with a measurement done after 120 min (Fig. 4e). The increase in activity in comparison to untreated cell lines indicates that the Curcumin binding to p53Y220C mutant restores its function to induce apoptosis.

3.11. Annexin V and PI staining

Using Annexin V in conjunction with Propidium iodide (PI) the cell viability, the apoptotic state, or necrotic state of BxPC-3 cell line in the presence of Curcumin was performed. The PI does not stain the living cells with the intact plasma membrane, but the late apoptotic and necrotic cells will display red fluorescence upon staining. The images of BxPC-3 cells were taken after 24 h of Curcumin treatment. Cells with 3 μM and 8 μM of Curcumin treatment showed blebbing and apoptotic bodies in comparison to untreated cells (Fig. 5). The Alexa flour 488 conjugated Annexin V and PI staining showed that when the cells were treated with 3 μM Curcumin concentration, 50% of the cells were found to be in an early apoptotic phase as they appear green on FITC filter and many cells were in the late apoptotic stage.

In contrast, cells treated with 8 μM Curcumin showed more apoptotic bodies in comparison to 3 μM and negative control (Fig. 5b). Based on the apoptotic assay, no apoptotic activity was observed in the untreated p53Y220C mutant BxPC-3 cells. However, the increased activity with the Curcumin-treated cells indicates that the mutant protein function is restored by the ligand binding.

4. Discussion

Clinically, it has been shown that Curcumin from the plant *Curcuma longa* inhibits cancer growth by activation of apoptosis and cell growth arrest pathways in the human cancer cells [26,34,50,81,82]. A dose of 8 g /day has been reported to be non-toxic in phase II evaluation for treating cancers [83]. Curcumin with two benzene rings containing polar groups is a pharmacologically safe natural compound and it can be used as a ligand to stabilize p53Y220C mutant to restore its function. The mutation of the residue Tyrosine 220 to Cysteine disturbs the hydrophobic core architecture located in the β-sandwich region. The crevice dimension between two S3/S4 and S7/S8 loops varies from 5.5 Å (C^{α}C220 - C^{α}T155) from one end with a maximum opening of 16 Å (C^{α}G226 - C^{α}S149) in the mid loop region to 5.3 Å (C^{α}C229 - C^{α}W146) (Table 3a and 3b). In wild type, eight water molecules (PDB ID: 2OCJ and 2IOI) were observed at the crevice whereas in p53Y220C structure (PDB ID:6SHZ) eleven water molecules were found [17] (Fig. S1b). The replacement of the residue Tyr to Cys leads to loss of network of hydrogen-bonded interactions stabilizing the S3/S4 and S7/S8 loops. The loops become flexible as the crevice has more solvent accessibility. Therefore, a ligand or a small molecule that could prevent the solvent accessibility and maintain the hydrophobic architecture will help in restoring the mutant to function like wild type. In this study, the Curcumin with a similar scaffold as other reported ligands [8,12,15–17,23,31,84] occupy the p53Y220C surface crevice with an estimated free energy of binding −9.92 kcal/mol. The Curcumin interacts with the S3/S4 and S7/S8 loops by forming six hydrogen-bonded interactions with the backbone atoms of the residues Leu145, Val147, Pro152, and Thr155 (Fig. 1b). The 100 ns MD simulations showed Curcumin remains bound inside the crevice stabilizing the loops with solvent observed in the crevice. Whereas, in the absence of Curcumin, the loops moved close to each other narrowing the space around one side of the crevice (Fig. 1e). The Curcumin binds p53Y220C (K_d = ~3 μM) and stabilizes the β-fold shown in IR and CD spectra (Fig. 3) to restore its function by increasing its affinity towards DNA. The p53Y220C gets stabilized by Curcumin shown by the appearance of bands at 1652 cm^{-1} (α-helices) and 1636 cm^{-1} (β-sheets) in the IR measurement (Fig. S2b). Curcumin holds the secondary structural elements of the domain and provides the plasticity to the protein to bind DNA shown by the IR spectra of Curcumin bound p53Y220C with DNA (Fig. 3d) where bands appeared at 1686 cm^{-1} (antiparallel β-sheets/turn), 1654 cm^{-1} (α-helices) and 1636 cm^{-1} (β-sheets) like wild type. The Curcumin binding increases the DNA binding affinity of p53 mutant by 4-fold from 3.5 μM to 0.8 μM. So, our biophysical studies establish that Curcumin binding stabilizes p53Y220C mutant to bind DNA with better affinity. A structural comparison was also performed with the PhiKans reported restoring the mutant function by binding to the crevice [8,12,15–17,23,31,84]. The structural analysis of PhiKans complexes showed all the compounds form four major hydrogen bonds with backbone atoms of Pro151, Leu145, Asp228, Thr150, and water-mediated hydrogen-bonded interactions with other loop residues. The PhiKans form hydrophobic interaction with Cys220 thus prevents the solvent entry and stabilizes the domain (Fig. S4c). The superposition of docked Curcumin with the PhiKans showed that the ligand occupies a similar position. Curcumin forms interactions like PhiKans with the backbone atoms and hydrophobic residues of loop S3/S4 and S7/S8 (Fig. S4a). Out of all reported ligands so far, the compound MB170 showed the best binding affinity of 4 μM [31], and Curcumin showed a comparable binding affinity of 3 μM. The Curcumin interactions with p53Y220DBD are also comparable to MB170 (Fig. S4b) with the five hydrogen-bonded and hydrophobic interactions with residues Leu145, Val147, Pro151, Thr155, and Cys220 maintained throughout 100 ns MD simulations (Fig. 1c–d). The MD trajectory of native p53Y220C in the absence of Curcumin showed more solvent molecules inside the core domain than the Curcumin docked complex. A comparison of the MD trajectory of p53Y220C in the absence and presence of Curcumin showed that the loop S3/S4 and S7/S8 of the complex were more stable in the presence of Curcumin than the native protein. In the absence of ligand, water molecules were observed in between the loop S3/S4 and S7/S8 destabilizing the fold at that region (Fig. 1e–f). The cell line-based experiments with the p53Y220C genomic mutant BxPC-3 pancreatic cancer cell line also showed that 3 μM Curcumin concentration could induce apoptosis shown by the COMET assay. By Annexin V and PI staining, we could observe an early apoptotic phase at 3 μM and late apoptotic phase along with apoptotic bodies at 8 μM concentration of Curcumin-treated cells. An increase in caspase-3 activity was observed in the BxPC-3 cells treated with 8 μM Curcumin indicating the activation of apoptotic pathway. Hence, based on our experimental data we propose that the apoptosis [83,85] and G2/M cell cycle arrest [86] pathways are activated by the functionally restored p53Y220C mutant in the pancreatic cancer cells. In healthy human pancreatic ductal epithelial cells (HPDE-6) Curcumin does not induce these pathways even at a higher concentration of 50 μM. The structurally non-functional p53 mutant could not activate the apoptotic pathways in the cancer cell lines. Upon addition of Curcumin, p53Y220C mutant gets stabilized and the number of functionally restored p53 increases. The kinases ATR, ATM, Chk1 and/Chk2 [14,85,87] (Fig. 5c) recognize the structurally restored p53Y220C and perform post-translational modifications to make p53Y220C functionally active. The active p53Y220C binds to the promoter sequence and initiates the gene transcription of apoptotic pathways shown by an increase in caspase-3 activity in the Curcumin-treated BxPC-3 cell lines [85]. We do agree that our hypothesis requires further studies to establish each step in the proposed mechanism.

5. Conclusion

Curcumin is documented as a therapeutic compound to prevent cancer by many clinical trial studies [29,50,88–90] which have shown that Curcumin inhibits the human pancreatic cell line harboring genomic mutant p53Y220C (BxPC-3) by the activation of G2/M cell cycle arrest and apoptotic kinases ATM/Chk1/Cdc25C. Our Biophysical studies establish that Curcumin stabilizes p53Y220C and restore its DNA binding efficiency. The cell lines experimental studies, Annexin V and caspase-3 assay indicates that the apoptotic and cell cycle pathway activation in BxPC-3 is mediated by functionally restored p53Y220C by Curcumin. The functionally restored p53Y220C activated by ATM/Chk1 kinases through PTM, which further enables the Apoptotic and cell cycle pathway genes, results in cleavage in caspase-3 and PARP. However, further studies are required to determine the mechanism of the signaling pathways mediated by Curcumin based functionally restored p53Y220C in human pancreatic cancer cells.

Supplementary data to this article can be found online at https://doi.org/10.1016/j.bbagen.2020.129807.

Ethical approval

The article does not involve any study with human participants or animals to be performed by any of the authors.

CRediT authorship contribution statement

Lakshay Malhotra: Investigation, Methodology, Writing - original draft, Writing - review & editing. **Harsh K.V. Goyal**: Investigation, Methodology. **Sunita Jhuria**: Investigation, Methodology. **Kapil Dev**: Resources. **Saroj Kumar**: Supervision, Validation, Visualization, Writing - review & editing. **Manoj Kumar**: Supervision, Validation, Visualization, Writing - review & editing. **Punit Kaur**: Software. **Abdul S. Ethayathulla**: Conceptualization, Formal analysis, Funding acquisition, Project administration, Resources, Supervision, Validation, Visualization, Writing - original draft, Writing - review & editing.

Declaration of Competing Interest

The authors have no substantial financial or commercial conflicts of interest with the current work or its publication.

Acknowledgments

The LM is thankful to the Department of Biotechnology (DBT) for providing the Junior Research Fellowship. Dr. A.S.E is thankful to All India Institute of Medical Sciences New Delhi, India for the Intramural Grant ID-A577.

References

[1] W.A. Freed-Pastor, C. Prives, Mutant p53: one name, many proteins, Genes Dev. 26 (2012) 1268–1286.
[2] P.A.J. Muller, K.H. Vousden, Mutant p53 in cancer: new functions and therapeutic opportunities, Cancer Cell 25 (2014) 304–317.
[3] B.D. Wallentine, et al., Structures of oncogenic, suppressor and rescued p53 core-domain variants: mechanisms of mutant p53 rescue, Acta Crystallogr. D Biol. Crystallogr. 69 (2013) 2146–2156.
[4] A.M. Goh, C.R. Coffill, D.P. Lane, The role of mutant p53 in human cancer, J. Pathol. 223 (2011) 116–126.
[5] A. Parrales, T. Iwakuma, Targeting oncogenic mutant p53 for Cancer therapy, Front. Oncol. 5 (2015).
[6] A. Ventura, et al., Restoration of p53 function leads to tumour regression in vivo, Nature 445 (2007) 661–665.
[7] A.B. Williams, B. Schumacher, p53 in the DNA-damage-repair process, Cold Spring Harb. Perspect. Med. 6 (2016).
[8] A.C. Joerger, A.R. Fersht, The p53 pathway: origins, inactivation in Cancer, and emerging therapeutic approaches, Annu. Rev. Biochem. (2016), https://doi.org/10.1146/annurev-biochem-060815-014710.
[9] A.C. Joerger, M.D. Allen, A.R. Fersht, Crystal structure of a superstable mutant of human p53 core domain. Insights into the mechanism of rescuing oncogenic mutations, J. Biol. Chem. 279 (2004) 1291–1296.
[10] G. Selivanova, K.G. Wiman, Reactivation of mutant p53: molecular mechanisms and therapeutic potential, Oncogene 26 (2007) 2243–2254.
[11] A.L. Okorokov, F. Ponchel, J. Milner, Induced N- and C-terminal cleavage of p53: a core fragment of p53, generated by interaction with damaged DNA, promotes cleavage of the N-terminus of full-length p53, whereas ssDNA induces C-terminal cleavage of p53, EMBO J. 16 (1997) 6008–6017.
[12] N. Basse, et al., Toward the rational design of p53-stabilizing drugs: probing the surface of the oncogenic Y220C mutant, Chem. Biol. 17 (2010) 46–56.
[13] V.J.N. Bykov, K.G. Wiman, Mutant p53 reactivation by small molecules makes its way to the clinic, FEBS Lett. 588 (2014) 2622–2627.
[14] K.G. Wiman, Pharmacological reactivation of mutant p53: from protein structure to the cancer patient, Oncogene 29 (2010) 4245–4252.
[15] A.C. Joerger, et al., Exploiting transient protein states for the Design of Small-Molecule Stabilizers of mutant p53, Struct. Lond. Engl. 1993 (23) (2015) 2246–2255.
[16] X. Liu, et al., Small molecule induced reactivation of mutant p53 in cancer cells, Nucleic Acids Res. 41 (2013) 6034–6044.
[17] M.R. Bauer, et al., Targeting cavity-creating p53 Cancer mutations with small-molecule stabilizers: the Y220X paradigm, ACS Chem. Biol. 15 (2020) 657–668.
[18] A. McGuigan, et al., Pancreatic cancer: a review of clinical diagnosis, epidemiology, treatment and outcomes, World J. Gastroenterol. 24 (2018) 4846–4861.
[19] L. Bouaoun, et al., *TP53* variations in human cancers: new lessons from the IARC TP53 database and genomics data: human mutation, Hum. Mutat. 37 (2016) 865–876.
[20] B. Leroy, et al., The TP53 website: an integrative resource Centre for the TP53 mutation database and TP53 mutant analysis, Nucleic Acids Res. 41 (2013) D962–D969.
[21] Shah Md Abdur Rauf, A. Endou, H. Takaba, A. Miyamoto, Effect of Y220C mutation on p53 and its rescue mechanism: a computer chemistry approach, Protein J. 32 (2013) 68–74.
[22] A.C. Joerger, H.C. Ang, A.R. Fersht, Structural basis for understanding oncogenic p53 mutations and designing rescue drugs, Proc. Natl. Acad. Sci. 103 (2006) 15056–15061.
[23] F.M. Boeckler, et al., Targeted rescue of a destabilized mutant of p53 by an in silico screened drug, Proc. Natl. Acad. Sci. 105 (2008) 10360–10365.
[24] M.R. Bauer, et al., A structure-guided molecular chaperone approach for restoring the transcriptional activity of the p53 cancer mutant Y220C, Future Med. Chem. 11 (2019) 2491–2504.
[25] G. Garcea, et al., Consumption of the putative chemopreventive agent curcumin by cancer patients: assessment of curcumin levels in the colorectum and their pharmacodynamic consequences, Cancer Epidemiol. Biomark. Prev. Publ. Am. Assoc. Cancer Res. Cosponsored Am. Soc. Prev. Oncol. 14 (2005) 120–125.
[26] R.A. Sharma, et al., Pharmacodynamic and pharmacokinetic study of oral Curcuma extract in patients with colorectal cancer, Clin. Cancer Res. Off. J. Am. Assoc. Cancer Res. 7 (2001) 1894–1900.
[27] M. Bayet-Robert, et al., Phase I dose escalation trial of docetaxel plus curcumin in patients with advanced and metastatic breast cancer, Cancer Biol. Ther. 9 (2010) 8–14.
[28] S. Vadhan-Raj, et al., Curcumin Downregulates NF-kB and related genes in patients with multiple myeloma: results of a phase I/II study, Blood 110 (2007) 1177.
[29] S. Durgaprasad, C.G. Pai, J.F. Vasanthkumar Alvres, S. Namitha, A pilot study of the antioxidant effect of curcumin in tropical pancreatitis, Indian J. Med. Res. 122 (4) (2005) 315–318.
[30] R. Epelbaum, M. Schaffer, B. Vizel, V. Badmaev, G. Bar-Sela, Curcumin and gemcitabine in patients with advanced pancreatic cancer, Nutr. Cancer 62 (2010) 1137–1141.
[31] M.G.J. Baud, et al., Aminobenzothiazole derivatives stabilize the thermolabile p53 cancer mutant Y220C and show anticancer activity in p53-Y220C cell lines, Eur. J. Med. Chem. 152 (2018) 101–114.
[32] A. Rahmani, M. Alsahli, S. Aly, M. Khan, Y. Aldebasi, Role of curcumin in disease prevention and treatment, Adv. Biomed. Res. 7 (2018) 38.
[33] M. Tomeh, R. Hadianamrei, X. Zhao, A review of Curcumin and its derivatives as anticancer agents, Int. J. Mol. Sci. 20 (2019) 1033.
[34] R. Wilken, M.S. Veena, M.B. Wang, E.S. Srivatsan, Curcumin: a review of anti-cancer properties and therapeutic activity in head and neck squamous cell carcinoma, Mol. Cancer 10 (2011) 12.
[35] P. Izetti, et al., PRIMA-1, a mutant p53 reactivator, induces apoptosis and enhances chemotherapeutic cytotoxicity in pancreatic cancer cell lines, Investig. New Drugs 32 (2014) 783–794.
[36] S. Banerjee, et al., Ancient drug curcumin impedes 26S proteasome activity by direct inhibition of dual-specificity tyrosine-regulated kinase 2, Proc. Natl. Acad. Sci. 115 (2018) 8155–8160.
[37] G.M. Morris, et al., AutoDock4 and AutoDockTools4: automated docking with selective receptor flexibility, J. Comput. Chem. 30 (2009) 2785–2791.
[38] G.S. Rao, M. Kumar, Structure-based design of a potent and selective small peptide inhibitor of *Mycobacterium tuberculosis* 6-hydroxymethyl-7, 8-dihydropteroate synthase: a computer modelling approach, Chem. Biol. Drug Des. 71 (2008) 540–545.
[39] F. Naz, et al., Drug repurposing approach to target FtsZ cell division protein from *Salmonella typhi*, Int. J. Biol. Macromol. 159 (2020). https://pubmed.ncbi.nlm.nih.gov/32417543/.

[40] M.J. Abraham, et al., GROMACS: high performance molecular simulations through multi-level parallelism from laptops to supercomputers, SoftwareX 1–2 (2015) 19–25.
[41] L.D. Schuler, X. Daura, W.F. van Gunsteren, An improved GROMOS96 force field for aliphatic hydrocarbons in the condensed phase, J. Comput. Chem. 22 (2001) 1205–1218.
[42] N. Schmid, et al., Definition and testing of the GROMOS force-field versions 54A7 and 54B7, Eur. Biophys. J. EBJ 40 (2011) 843–856.
[43] P. Yadav, M. Kumar, R. Bansal, P. Kaur, A.S. Ethayathulla, Structure model of ferrochelatase from Salmonella Typhi elucidating metalation mechanism, Int. J. Biol. Macromol. 127 (2019) 585–593.
[44] A. Micsonai, et al., BeStSel: a web server for accurate protein secondary structure prediction and fold recognition from the circular dichroism spectra, Nucleic Acids Res. 46 (2018) W315–W322.
[45] A. Micsonai, et al., Accurate secondary structure prediction and fold recognition for circular dichroism spectroscopy, Proc. Natl. Acad. Sci. 112 (2015) E3095–E3103.
[46] H.A. Tajmir-Riahi, C.N. N'soukpoé-Kossi, D. Joly, Structural analysis of protein–DNA and protein–RNA interactions by FTIR, UV-visible and CD spectroscopic methods, Spectroscopy 23 (2009) 81–101.
[47] K.K. Gupta, S.S. Bharne, K. Rathinasamy, N.R. Naik, D. Panda, Dietary antioxidant curcumin inhibits microtubule assembly through tubulin binding, FEBS J. 273 (2006) 5320–5332.
[48] S.A. Marathe, et al., Curcumin reduces the motility of *Salmonella enterica* Serovar typhimurium by binding to the flagella, Thereby Leading to Flagellar Fragility and Shedding, J. Bacteriol. 198 (2016) 1798–1811.
[49] D. Rai, J.K. Singh, N. Roy, D. Panda, Curcumin inhibits FtsZ assembly: an attractive mechanism for its antibacterial activity, Biochem. J. 410 (2008) 147–155.
[50] A. Sahu, N. Kasoju, U. Bora, Fluorescence study of the Curcumin−casein micelle Complexation and its application as a drug Nanocarrier to Cancer cells, Biomacromolecules 9 (2008) 2905–2912.
[51] M.K. Danks, D.O. Whipple, C.R. McPake, D. Lu, L.C. Harris, Differences in epitope accessibility of p53 monoclonal antibodies suggest at least three conformations or states of protein binding of p53 protein in human tumor cell lines, Cell Death Differ. 5 (1998) 678–686.
[52] X. Su, et al., Effect of p53 on pancreatic cancer-glucose tolerance abnormalities by regulating transglutaminase 2 in resistance to glucose metabolic stress, Oncotarget 8 (2017) 74299–74311.
[53] L. Florento, et al., Comparison of cytotoxic activity of anticancer drugs against various human tumor cell lines using in vitro cell-based approach, Int. J. Biomed. Sci. IJBS 8 (2012) 76–80.
[54] P.L. Olive, J.P. Banáth, The comet assay: a method to measure DNA damage in individual cells, Nat. Protoc. 1 (2006) 23–29.
[55] M.I. Ahmad, M.F. Zafeer, M. Javed, M. Ahmad, Pendimethalin-induced oxidative stress, DNA damage and activation of anti-inflammatory and apoptotic markers in male rats, Sci. Rep. 8 (2018) 17139.
[56] G.A. Husseini, K.L. O'Neill, W.G. Pitt, The comet assay to determine the mode of cell death for the ultrasonic delivery of doxorubicin to human leukemia (HL-60 cells) from pluronic P105 micelles, Technol. Cancer Res. Treat. 4 (2005) 707–711.
[57] B.M. Gyori, G. Venkatachalam, P.S. Thiagarajan, D. Hsu, M.-V. Clement, OpenComet: an automated tool for comet assay image analysis, Redox Biol. 2 (2014) 457–465.
[58] R. Yosef, et al., p21 maintains senescent cell viability under persistent DNA damage response by restraining JNK and caspase signaling, EMBO J. 36 (2017) 2280–2295.
[59] A. Samba-Louaka, et al., *Listeria monocytogenes* dampens the DNA damage response, PLoS Pathog. 10 (2014).
[60] E. Brauchle, S. Thude, S.Y. Brucker, K. Schenke-Layland, Cell death stages in single apoptotic and necrotic cells monitored by Raman microspectroscopy, Sci. Rep. 4 (2015) 4698.
[61] A.P. Demchenko, Beyond annexin V: fluorescence response of cellular membranes to apoptosis, Cytotechnology 65 (2013) 157–172.
[62] K. Fujimori, D. Ohta, An Arabidopsis cDNA encoding a bifunctional glutamine amidotransferase/cyclase suppresses the histidine auxotrophy of a *Saccharomyces cerevisiae* his7 mutant, FEBS Lett. 428 (1998) 229–234.
[63] R. Singh, S. Pervin, G. Wu, G. Chaudhuri, Activation of caspase-3 activity and apoptosis in MDA-MB-468 cells by Nω-hydroxy-L-arginine, an inhibitor of arginase, is not solely dependent on reduction in intracellular polyamines, Carcinogenesis 22 (2001) 1863–1869.
[64] S.-F. Lin, J.-D. Lin, C. Hsueh, T.-C. Chou, R.J. Wong, Activity of roniciclib in medullary thyroid cancer, Oncotarget 9 (2018) 28030–28041.
[65] X.-B. Liu, et al., G-protein signaling abnormalities mediated by CD95 in salivary epithelial cells, Cell Death Differ. 7 (2000) 1119–1126.
[66] Y. Cho, S. Gorina, P.D. Jeffrey, N.P. Pavletich, Crystal structure of a p53 tumor suppressor-DNA complex: understanding tumorigenic mutations, Science 265 (1994) 346–355.
[67] Y. Chen, R. Dey, L. Chen, Crystal structure of the p53 core domain bound to a full consensus site as a self-assembled tetramer, Struct. Lond. Engl. 1993 (18) (2010) 246–256.
[68] C. Chen, N. Gorlatova, Z. Kelman, O. Herzberg, Structures of p63 DNA binding domain in complexes with half-site and with spacer-containing full response elements, Proc. Natl. Acad. Sci. 108 (2011) 6456–6461.
[69] A.S. Ethayathulla, et al., Structure of p73 DNA-binding domain tetramer modulates p73 transactivation, Proc. Natl. Acad. Sci. U. S. A. 109 (2012) 6066–6071.
[70] A.S. Ethayathulla, H.T. Nguyen, H. Viadiu, Crystal structures of the DNA-binding domain tetramer of the p53 tumor suppressor family member p73 bound to different full-site response elements, J. Biol. Chem. 288 (2013) 4744–4754.
[71] A. Volkamer, D. Kuhn, T. Grombacher, F. Rippmann, M. Rarey, Combining global and local measures for structure-based druggability predictions, J. Chem. Inf. Model. 52 (2012) 360–372.
[72] B.J. Anderson, C. Larkin, K. Guja, J.F. Schildbach, Using Fluorophore-labeled oligonucleotides to measure affinities of protein-DNA interactions, Methods Enzymol. 450 (2008) 253–272.
[73] W.C. Johnson, Analyzing protein circular dichroism spectra for accurate secondary structures, Proteins Struct. Funct. Genet. 35 (1999) 307–312.
[74] G. Böhm, R. Muhr, R. Jaenicke, Quantitative analysis of protein far UV circular dichroism spectra by neural networks, Protein Eng. Des. Sel. 5 (1992) 191–195.
[75] N.J. Greenfield, Using circular dichroism spectra to estimate protein secondary structure, Nat. Protoc. 1 (2006) 2876–2890.
[76] A. Barth, Infrared spectroscopy of proteins, Biochim. Biophys. Acta 1767 (2007) 1073–1101.
[77] H. Yang, S. Yang, J. Kong, A. Dong, S. Yu, Obtaining information about protein secondary structures in aqueous solution using Fourier transform IR spectroscopy, Nat. Protoc. 10 (2015) 382–396.
[78] E.L. Deer, et al., Phenotype and genotype of pancreatic cancer cell lines, Pancreas 39 (2010) 425–435.
[79] R. Weinel, J. Schmidt, Frequent alterations of the tumor suppressor genes ~53 and DCC in human pancreatic carcinoma, Gastroentology 106 (1994) 7.
[80] J. Häcki, et al., Apoptotic crosstalk between the endoplasmic reticulum and mitochondria controlled by Bcl-2, Oncogene 19 (2000) 2286–2295.
[81] Y.S. Tan, Y. Mhoumadi, C.S. Verma, Roles of computational modelling in understanding p53 structure, biology, and its therapeutic targeting, J. Mol. Cell Biol. (2019), https://doi.org/10.1093/jmcb/mjz009.
[82] M. Sun, et al., Curcumin (diferuloylmethane) alters the expression profiles of microRNAs in human pancreatic cancer cells, Mol. Cancer Ther. 7 (2008) 464–473.
[83] R.A. Sharma, et al., Phase I clinical trial of oral curcumin: biomarkers of systemic activity and compliance, Clin. Cancer Res. Off. J. Am. Assoc. Cancer Res. 10 (2004) 6847–6854.
[84] D. Sundar, et al., Wild type p53 function in p53Y220C mutant harboring cells by treatment with Ashwagandha derived anticancer withanolides: bioinformatics and experimental evidence, J. Exp. Clin. Cancer Res. CR 38 (2019).
[85] R.P. Sahu, S. Batra, S.K. Srivastava, Activation of ATM/Chk1 by curcumin causes cell cycle arrest and apoptosis in human pancreatic cancer cells, Br. J. Cancer 100 (2009) 1425–1433.
[86] W.R. Taylor, G.R. Stark, Regulation of the G2/M transition by p53, Oncogene 20 (2001) 1803–1815.
[87] G. Lossaint, E. Besnard, D. Fisher, J. Piette, V. Dulić, Chk1 is dispensable for G2 arrest in response to sustained DNA damage when the ATM/p53/p21 pathway is functional, Oncogene 30 (2011) 4261–4274.
[88] T.-W. Tan, et al., Curcumin-induced cell cycle arrest and apoptosis in human acute promyelocytic leukemia HL-60 cells via MMP changes and caspase-3 activation, Anticancer Res. 26 (2006) 4361–4371.
[89] N. Dhillon, et al., Phase II trial of curcumin in patients with advanced pancreatic Cancer, Clin. Cancer Res. 14 (2008) 4491–4499.
[90] Y. Li, et al., Salvation of the fallen angel: reactivating mutant p53, Br. J. Pharmacol. 176 (2019) 817–831.
[92] Brian J. Anderson, Chris Larkin, Kip Guja, Joel F. Schildbach, Using fluorophore-labeled oligonucleotides to measure affinities of protein-DNA interactions, Methods Enzymol. 450 (2008) 253–272, https://doi.org/10.1016/S0076-6879(08)03412-5.